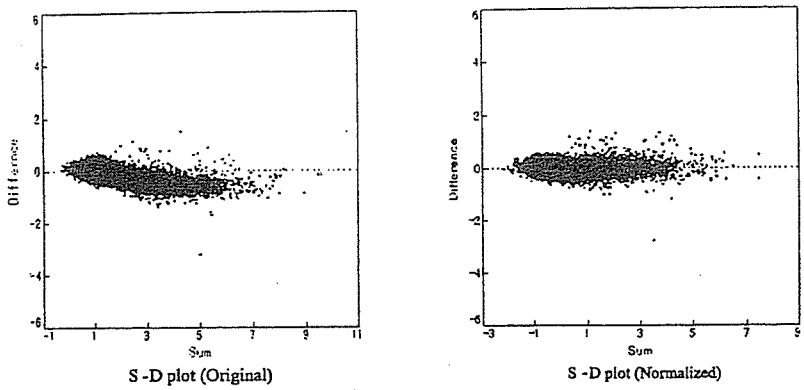

Fig. 5. The S-D plot of original data is shown on the left, and that of normalized data on the right.

$\mu_0 < \mu_1$ and $0 < \xi < 1$.

Figure 6(a) shows the comparison of the fitted mixed normal distribution function with two components (pink line) and the empirical cumulative distribution (brown line). The red line shows the distribution of expression intensities of (ON, ON) genes, the blue line the distribution of expression intensities of (OFF, OFF) genes, and the lime line the distribution of expression intensities of (ON, OFF) or (OFF, ON) genes. Figure 6(b) shows the corresponding density functions.

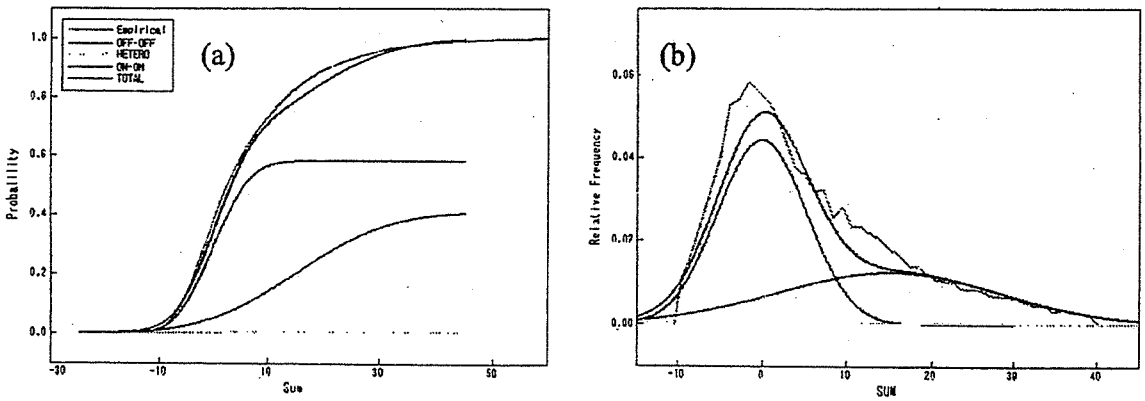

Fig. 6. (a) The estimated mixed normal distribution with two components is shown by the pink line. The distribution of expression intensities of (ON, ON) genes is shown by the red line, that of (OFF, OFF) genes by the blue line and that of (ON, OFF) or (OFF, ON) genes by the lime line. The cumulative distribution of empirical data is shown by the brown line. (b) The density functions corresponding to each distribution function. (See the colored figure given later)

Step E2. Estimate the unknown parameters μ, λ^2, σ_β^2 and σ_ε^2 using the following formula:

$$\hat{\mu} = \frac{\mu_1 - \mu_0}{2}, \quad \hat{\sigma_\varepsilon^2} = \frac{1}{2||\{i|\ u_i < \hat{\mu_0}\}||} \sum_{i \in \{i|\ u_i < \hat{\mu_0}\}} v_i^2,$$

$$\hat{\sigma_\beta^2} = \frac{1}{4}\hat{\sigma_0^2} - \frac{1}{2}\hat{\sigma_\varepsilon^2}, \quad \text{and} \quad \hat{\lambda^2} = \log\left(1 + \frac{\hat{\sigma_1^2} - \hat{\sigma_0^2}}{4\hat{\mu}^2}\right).$$

Step E3. Given $\hat{\theta} = (\hat{\mu}, \hat{\lambda^2}, \hat{\sigma_\beta^2}, \hat{\sigma_\varepsilon^2})$, fit the following mixed normal model with four components to the data $\{(u_i, v_i),\ i = 1, \cdots, n\}$:

$$\begin{aligned}
&p_{00}\phi(u|4\hat{\sigma_\beta^2} + 2\hat{\sigma_\varepsilon^2})\phi(v|2\hat{\sigma_\varepsilon^2}) \\
&+ p_{10}\phi_2(u - \hat{\mu}, v - \hat{\mu}|\hat{\Sigma_{10}}) + p_{01}\phi_2(u - \hat{\mu}, v + \hat{\mu}|\hat{\Sigma_{01}}) \\
&+ (1 - p_{00} - p_{10} - p_{01})\phi(u - 2\mu|4\hat{\mu}^2(e^{\hat{\sigma_\alpha^2}} - 1) + 4\hat{\sigma_\beta^2} + 2\hat{\sigma_\varepsilon^2})\phi(v|2\hat{\sigma_\varepsilon^2}).
\end{aligned}$$

Then calculate the tentative maximum likelihood estimate $\hat{\boldsymbol{p}} = (\hat{p}_{00}, \hat{p}_{10}, \hat{p}_{01}, \hat{p}_{11})$ of $\boldsymbol{p}$.

Step E4. Given $\hat{\mathbf{p}} = (\hat{p}_{00}, \hat{p}_{10}, \hat{p}_{01}, \hat{p}_{11})$, fit the following mixed normal model with four components to the data $\{(u_i, v_i),\ i = 1, \cdots, n\}$,

$$\begin{aligned}
&\hat{p}_{00}\phi(u|4\sigma_\beta^2 + 2\sigma_\varepsilon^2)\phi(v|2\sigma_\varepsilon^2) \\
&+ \hat{p}_{10}\phi(u - \mu, v - \mu|\Sigma_{10}) + \hat{p}_{01}\phi_2(u - \mu, v + \mu|\Sigma_{01}) \\
&+ \hat{p}_{11}\phi_2(u - 2\mu|4\mu^2(e^{\sigma_\alpha^2} - 1) + 4\sigma_\beta^2 + 2\sigma_\varepsilon^2)\phi(v|2\sigma_\varepsilon^2).
\end{aligned}$$

Then calculate the tentative maximum likelihood estimate $\hat{\boldsymbol{\theta}} = (\hat{\mu}, \hat{\lambda^2}, \hat{\sigma_\beta^2}, \hat{\sigma_\varepsilon^2})$ of $\boldsymbol{\theta}$. Iterate step E3 and E4 to convergence.

We obtain the estimates $\hat{\boldsymbol{\theta}} = (7.55,\ 0.64,\ 6.35,\ 0.96)$ and $\hat{\boldsymbol{p}} = (0.582,\ 0.004, 0.004,\ 0.410)$ with the normalized sample data. Given $\hat{\boldsymbol{p}}$, $\hat{\boldsymbol{\theta}}$ and the normalized sample data, the degree to which a gene is expressed differentially in the two samples is quantified by the posterior probabilities in (11). The colored S-D plot for normalized sample data is shown in Figure 7. Each color indicates the magnitude of probability: blue represents 0.0 to 0.2, light blue 0.2 to 0.4, yellow 0.4 to 0.6, magenta 0.6 to 0.8 and red 0.8 to 1.0.

4. Discussion

So far several statistical approaches have been made to identify the important genes amongst the many that are measured. Inference about differential gene expression between two cell types is typically based on the difference of measurements between channels 1 and 2 (or the ratio if the logarithmic transformation is used). We adopted two key distinctions of the present approach from earlier efforts. First we introduced the concept of the binary states of gene expressions, "ON" and "OFF", which yields the simple mathematical modeling. The model suggests that the large difference of gene expression intensities between channels 1 and 2 does not always gives

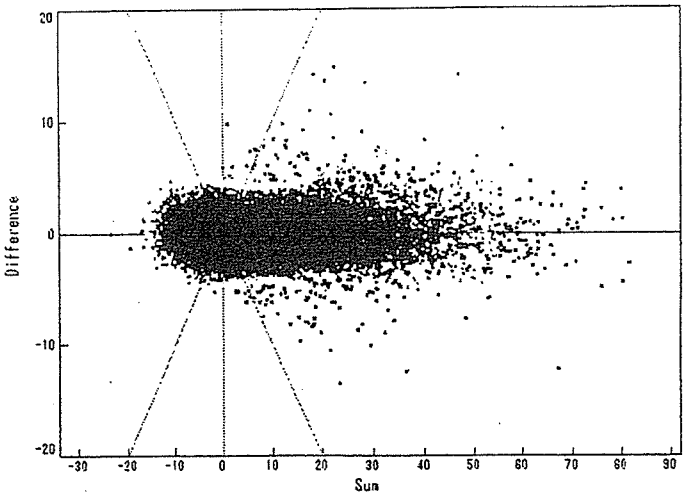

Fig. 7. Each color indicates the magnitude of the posterior probability of a gene expressed differentially in the two samples. Dark blue represents 0.0 to 0.2, light blue 0.2 to 0.4, green 0.4 to 0.6, yellow 0.6 to 0.8 and red 0.8 to 1.0. (See the colored figure given later)

a significant difference, because when its status is (ON, ON), the difference has no meaning. Actually it may be over-simplification to quantify gene expression level using a binary latent variable. A more detailed model may be needed for analyzing the gene expression data in future. However, no high-throughput method is available for discriminating multi-levels more than two for positive expression of gene. Therefore we use the binary latent variable model in microarray data analysis for the present.

The other key distinction of our approach is using the "sum" and "difference" of gene expression intensities of the two samples simultaneously. Several reports have indicated that the magnitude of the difference can have a systematic dependence on overall intensity. Dudoit et al. (2002) described that the plot of $M = \log_2(CH1/CH2)$ vs. $A = \log_2 \sqrt{CH1 * CH2}$, called an MA-plot, clearly showed dependence of the log ratio M on overall spot intensity A. Quackenbush (2002) used a plot similar to the MA-plot. He proposed that the easiest way to visualize the intensity dependent effect is to plot $R = \log_2(CH1/CH2)$ vs. $I = \log_{10}(CH1 * CH2)$, and used this plot for removing the intensity dependent error. In this study, we characterized a gene by the joint "sum" and "difference" of its expression intensities in two samples and applied a two-dimensional mixed normal model with four components. Figure 2 illustrates our model. The genes of interest to us belong to regions C and D, where V reflects the true difference of expression intensity between the two samples. On the contrary, genes belonging to regions A and B are not informative, because V reflects only measurement error. If there exists no common variation between the two cells, then the variances of "sum" and "difference" are expected to be same for the component (OFF, OFF), yielding a spherical shape of scatter plot should appear at the region A in SD-plot after normalization, which makes us easy to check visually degree of the performance of normalization.

One major source of variation is the background intensities. Yoon et al. (2004) stressed the importance of adjusting the effect of the background intensities in the normalization process and concluded that the background measure $\log y_i^{(\ell)} - \log b_i^{(\ell)}$ performs well in their normalization process. As for Affymetrix GeneChip probe level data, Irizarry et al. (2003) stated that the subtraction $PM - MM$ as a way of correcting for non-specific binding is not appropriate and proposed the expression measures based on a log scale linear additive model (RMA). Our approach is similar to theirs. To avoid the quantity $y_i^{(\ell)} - b_i^{(\ell)}$ taking on negative values, we adopt the equation (12) to correct background effects. The nonparametric regression model $\log y_i^{(\ell)} = \phi(\log b_i^{(\ell)}) + \varepsilon_i$, where $E(\varepsilon_i) = 0$, may be applicable to the background correction, but it usually does not work well because of over-fit the data according to our experience. Figure 8 is the scatter diagram of $(\log y_i, \log b_i)$, in which the regression coefficient is close to 1.0 (0.77). The assumption that the foreground intensity is in proportion to the background intensity seems to be appropriate.

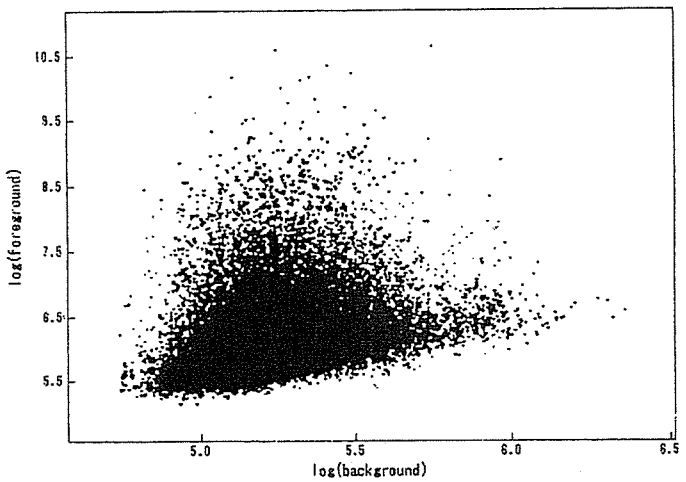

Fig. 8. Scatter diagram of pairs of background and foreground intensities. It shows a tendency towards stronger background intensity with stronger foreground intensity. The calculated regression coefficient is 0.77.

There are many approaches to normalizing expression levels. Dudoi et al. (2002) stated that the usual global normalization approaches are not adequate to remove intensity -or spatially-dependent dye biases. They applied the lowess smoother to each subgrid to remove them. Our approach, though similar to theirs, is not quite the same. The main difference is that we consider the location of a subgrid on a slide and the location of a spot on a subgrid. By Step N1, biases associated with the location of subgrids on a slide can be accommodated. We give a detailed explanation of this in 'Adjustment among subgrids'. Step N2 accounts for the removal of the biases associated with a two-dimensional location of a spot on a subgrid. We try to minimize them using the multiple nonparametric regression model with coordinates of the spot as explanatory variables. Biases linked to the different efficiencies of the two dyes are minimized by Step N3.

[Adjustment among subgrids]

It is natural to assume that most of the genes in a microarray are similarly expressed in the query and reference samples ((OFF, OFF) or (ON, ON)), whereas only a small fraction of genes are differentially expressed ((ON, OFF) or (OFF, ON)). Most of the pairs (u_i, v_i) are presumed to be generated from the two-dimensional normal mixture distribution having components ((ON, ON) and (OFF, OFF)), where the values v_i show only measurement error. Based on this assumption, we adjust the (u_i, v_i)'s among subgrids. Assuming the DNA probes are spotted randomly on the glass slide, we can regard the data set $\{u_k(i.j)\}$ of an arbitrary subgrid k as random samples from the normal mixture distribution with components ((ON, ON) and (OFF, OFF)). If there is no bias depending on location of the subgrid, the values $Q_k^{(u)}(35)$ (35% point of $\{u_{(k)}(i, j)|i = 1, \cdots, 12. j = 1, \cdots, 12\}$) should have approximately the same value regardless of k. This percentile point depends on the mixture proportion of the two components. If, for example, the mixture proportion is one or zero, namely a single component, the median value (50% point) is the most stable point for the subgrids. The following simulation study supports empirically that the 35% point of $\{u_{(k)}(i, j)|i = 1, \cdots, 12, j = 1, \cdots, 12\}$ can be regarded as the most stable point.

Thirty thousand simulated data sets $\{u_i|i = 1, \cdots, 441\}$ were generated based on model (1), i.e. a gene being "ON" was generated from the log normal density function with mean $\log\mu - \frac{\lambda^2}{2}$ and variance λ^2 and a gene being "OFF" from the normal density function with mean 0 and variance σ_ε^2. The parameters $(\mu, \lambda, \sigma_\beta^2, \sigma_\varepsilon^2)$ were set to (0.5, 0.8, 0.2, 0.1). The mixture proportion of the two components was varied from 0.1 to 0.5 in intervals of 0.1. The standard deviations of each percentile point for each mixture proportion are shown in Figure 9. It demonstrates the

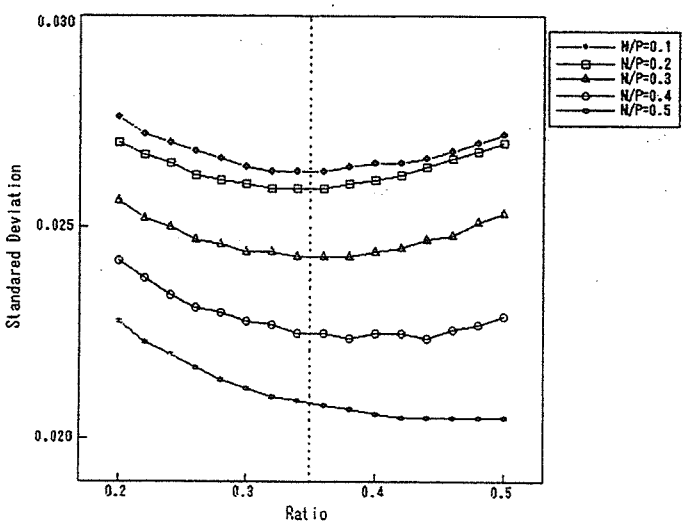

Fig. 9. The standard deviations of the percentile points from thousands of simulated data sets are shown. Blue, light blue, green, yellow, and red show the values for mixture proportions of 0.1, 0.2, 0.3, 0.4 and 0.5.

validity of taking the 35 % point, as it is the most stable.

Acknowledgements

The present study was supported by grants from the New Energy and Industrial Technology Development Organization and the Ministry of Education, Culture, Sports, Science and Technology. We thank Dr. Okazaki and Dr. Hayashizaki, Riken Yakohama Institute, for providing their microarray data. We are grateful to Dr. Cologne, Radiation Effects Research Foundation, for his reading of the manuscript. We thank the editor and two unnamed referees for helpful comments on a previous draft that led to substantial improvement of the manuscript.

REFERENCES

Arcana, IM. and Ohtaki, M.(2005). Multi-target models and their application to data analysis of cellular mortality due to radiation exposure. *Hiroshima Journal of Medical Science* **9(20)**

Baldi, P.and Lond, D. (2001). A Bayesian framework for the analysis of microarray expression data: regularized t-test and statistical inferences of gene changes. *Bioinformatics* **17(6)**, 509-519.

Box, GPE. and Cox DR. (1964). An analysis of transformation (with discussion). *Journal of the Royal Statistical Society* **B26**, 211-252.

Breiman, L. and Friedman, JH. (1985). Estimating optimal transformations for multiple regression and correlation, (with discussion). *Journal of American Statistical Association* **80**, 580-598.

Butte, A. (2002). The use and analysis of microarray data. *Nature Publishing Group* **1**, 951-960.

Churchill, GA. (2002). Fundamentals of experimental design for cDNA microarray. *Nature Genetics Supplement* **32**, 490-495.

Dudoit, S., Yang, YH., Callow, MJ.and Speed, TP. (2000). Statistical methods for identifying differentially expressed genes in replicated cDNA microarray experiments. *Technical Report* #578

Eisen, M. (1999). Scan Analyze User Manual.
http//rana.lbl.gov/manuals/ScanAnalyzeDoc.pdf

Fan, J., Tam, P., Woude, GV. and Ren, Y.(2004). Normalization and analysis of cDNA microarrays using within-array replications applied to neuroblastoma cell response to a cytokine. *Proceedings of the National Academy of Sciences* **101**, 1135-1140.

Gerhold, DL., Jensen, RV. and Gullans, SR. (2002). Better therapeutics through microarrays. *Nature Genetics. Supplement* **32**, 547-552.

Irizarry, R., Hobbs, B., Collin, F., Beazer-Barclay, YD., Antonellis, JK., Scherf, U. and Speed,T. (2003). Exploration, normalization, and summaries of high density oligonucleotide array probe level data. *Biostatistics* **4-2**, 249-264.

Irizarry, RA., Bolstad, BM., Collin F., Cope, LM., Hobbs, B., Speed, TP. (2003). Summaries of Affymetrix GeneChips probe level data. *Nucleic Acids Research* **31(4)**, e15.

Kerr, MK., Martin, M. and Churchill, GA. (2000). Analysis of variance for gene expression microarray data. *Journal of Computational Biology* **7-6**, 819-837.

Kendziorski, CM., Newton, MA., Lan, H.and Gould, MN. (2003). On parametric empirical Bayes methods for comparing multiple groups using replicated gene expression profiles. *Statistics in Medicine* **22**, 3899-3914.

Lee, MLT., Kuo, FC., Whitmore, GA. and Sklar, J.(2000). Importance of replication in microarray gene expression studies: Statistical method and evidence from repetitive cDNA hybridization. *Proceedings of the National Academy of Sciences* **97**, 9834-9839.

Li, C.and Wong, WH. (2001). Model-based analysis of oligonucleotide arrays: Expression index computation and outlier detection. *Proceedings of the National Academy of Sciences* **98(1)**, 31-36.

Long, AD., Mangalam, HJ., Chan, BYP., Tolleri, L., Hatfield, GW. and Baldi, P. (2001). Improved statistical inference from DNA microarray data using analysis of variance and a Bayesian statistical framework. Analysis of global gene expression in Escherichia Coli K12. *The Journal of Biological Chemistry* **276-23**, 19937-19944.

Newton, MA., Kendziorski, CM., Richmond, CS. and Blatner FR. (2001). On differential variability of expression ratios: Improving statistical inference about gene expression changes from microarray data. *Journal of Computational Biology* **8(1)**, 37-52.

Quackenbush, J.(2002). Microarray data normalization and transformation. *Nature Genetics Supplememt* **32**, 496-501.

Saviozzi, S.and Caogero, RA. (2003). Microarray probe expression measures, data normalization and statistical validation. *Comparative and functional genomics* **4**, 442-446.

Schena, M., Shalon, D., Davis, RW. and Brown, PO.(1995). Quantitative monitoring of gene expression patterns with a complementary DNA microarray. *Science* **270**, 467-470.

Schudhhardt, J., Beule, D., Malik, A., Wolski, E., Eickhoff, H., Lehrach, H. and Herzel, H. (2002). Normalization strategies for cDNA microarrays. *Nucleic Acid Research* **28(10)**, e47.

Yang, YH., Dudoit, S., Luu, P., Lin, DM., Peng, V., Nagai, J. and Speed, TP. (2002). Normalization for cDNA microarray data: a robust composite method addressing single and multiple slide systematic variation. *Nucleic Acid Research* **30(4)**, e15.

Yoon, D., Yi, SD., Kim, JH., Park, T. (2004). Two-stage normalization using background intensities in cDNA microarray data. *BMC Bioinformatics* **5**(1), 97.

Wu, W., Wildsmith, SE., Winkley, AJ., Yallop, R., Elock, FJ. and Bugelski, PJ. (2001). Chemometric strategies for normalization of gene expression data obtained from cDNA microarrays. *Analytica Chimica Acta* **466**, 451-466.

International Journal of
HEMATOLOGY

The Maturation of Myeloma Cells Correlates with Sensitivity to Chemotherapeutic Agents

Yoshiaki Kuroda,[a] Akira Sakai,[a] Yoshiko Okikawa,[a] Shoso Munemasa,[a] Yuta Katayama,[a] Hideo Hyodo,[a] Jun Imagawa,[b] Yasuo Takimoto,[b] Hajime Okita,[b] Megu Ohtaki,[c] Akiro Kimura[a]

Departments of [a]Hematology and Oncology and [c]Environmetrics and Biometrics, Research Institute for Radiation Biology and Medicine, Hiroshima University, Hiroshima; [b]Internal Medicine, Otake National Hospital, Otake, Japan

Received November 30, 2004; received in revised form February 3, 2005; accepted February 4, 2005

Abstract

We analyzed both morphologic and phenotypic findings of myeloma cells before and after chemotherapy in 21 patients with multiple myeloma. The morphologic analysis was based on the Greipp classification, and phenotypic analysis was performed by 3-color flow cytometry using the CD38 plasma gating method (Marrow plasma 38). Results with flow cytometry using a combination of MPC1, CD49e, and CD45 supported the morphologic findings for the myeloma cells. Treatment with 3 or 4 cycles of VAD (vincristine, doxorubicin, and dexamethasone) therapy was effective in reducing the total numbers of myeloma cells, but the proportion of immature myeloma cells increased after this treatment. However, the immature myeloma cells were reduced by high-dose melphalan (HD-Mel) therapy followed by autologous stem cell transplantation (ASCT). High-dose cyclophosphamide treatment for stem cell harvesting did not show an effect on the residual immature myeloma cells after VAD treatment. In addition, thalidomide was not effective in reducing the numbers of immature myeloma cells. These results suggest that VAD (3 or 4 cycles) therapy plus HD-Mel followed by ASCT is a reasonable treatment for multiple myeloma and that Marrow plasma 38 analysis is a useful method for monitoring the response of multiple myeloma to chemotherapy.
Int J Hematol. 2005;81:335-341. doi: 10.1532/IJH97.04189

Key words: Greipp classification; MPC1; CD49e; CD45; Myeloma cells

1. Introduction

Multiple myeloma (MM) is the result of a clonal proliferation of plasma cells, but myeloma cells have been shown to be heterogeneous with regard to their morphology and biological character. Recently, correlations between molecular subtypes and prognoses have been identified, such as a good prognosis with t(11;14) and a poor prognosis with t(4;14) and with t(14;16) [1] in addition to chromosome 13 abnormalities. However, how these molecular events affect the prognosis of MM patients is still unclear. In addition, it is difficult to analyze the heterogeneity of myeloma cells in each case of MM by molecular analysis. Twenty years ago, Greipp et al classified myeloma cells as mature, intermediate, immature, and plasmablastic [2], and they showed that the plasmablastic morphology is an independent predictor of poor survival rate after autologous stem cell transplantation (ASCT) [3]. On the other hand, Kawano et al classified myeloma cells according to phenotype into the following 3 types [4,5]: immature ($MPC1^-CD49e^-CD45^{-/+}$), intermediate ($MPC1^+CD49e^-CD45^-$), and mature ($MPC1^+CD49e^{+/-}CD45^+$). This phenotype-based classification shows a good correlation with that based on morphology. These authors also demonstrated that only a few subpopulations of tumor cells, such as $CD45^+MPC1^-CD49^-$ immature myeloma cells, proliferated in response to interleukin 6 [6]. Here we report our morphologic and phenotypic analyses of myeloma cells before and after chemotherapy to determine how these heterogeneous populations of myeloma cells change in response to some standard treatments.

Correspondence and reprint requests: Akira Sakai, MD, Department of Hematology and Oncology, Division of Clinical Research, Research Institute for Radiation Biology and Medicine, Hiroshima University, 1-2-3 Kasumi, Minami-ku Hiroshima 734-8553, Japan; 81-82-257-5861; fax: 81-82-256-7108 (e-mail: sakira@hiroshima-u.ac.jp).

2. Patients and Methods

2.1. Patients

Twenty-one patients with MM were studied. Their characteristics are shown in Table 1-1. The clinical staging was

Table 1-1.
Characteristics of the Patients and the Percentages of Myeloma Cell Types Based on Greipp Morphology before and after Chemotherapies*

Case No.	Sex	Age	CS	Type	Chemotherapy Regimen	Greipp Morphology: Mature/Intermediate/Immature, % (BM Plasma Cells, %) Serum† or Urinary‡ M Component: MP	VAD	HD-CPA	HD-Mel	Thalidomide
1	M	71	IIIB	BJ-λ	MP × 10	4/16/80 (12.5) 875‡	24/32/44 (1.5)§ 330‡			
2	M	80	IIIA	IgG/BJP-κ	MP × 12	6/33/61 (26) 4820†	12/48/40 (5.5)§ 2850†			
3	M	60	IIIB	IgG-κ	VAD × 4		19/50/31 (49) 6380†	4/14/82 (9)§‖ 1510†		
4	F	66	IIA	IgG-κ	VAD × 2		1/10/89 (2.5) 5540†	2/17/81 (1) 1340†		
5	M	56	IIIA	IgG-λ	VAD × 3		7/41/52 (12) 8480†	9/30/61 (5)§‖ 6580†		
6	M	70	IIIA	IgA/BJP-κ	VAD × 4		13/64/23 (21) 4660†	10/12/78 (11.5)§‖ 2320†		
7	F	70	IIIA	IgG-κ, IgG-λ	VAD × 2		4/60/36 (13.5) 3420†	20/32/48 (2.5)§‖ 1560†		
8	F	60	IIA	BJ-λ	VAD × 4 → HD-CPA		10/42/48 (24.5) 1950‡	2/22/76 (4.5)§‖ 524‡	4/20/76 (14.5) 399‡	
9	M	54	IIIA	IgA/BJP-κ	VAD × 3 → HD-CPA → HD-Mel		0/64/36 (70) 5550†	6/48/46 (7)§‖ 2500†	4/45/51 (9.5)§ 2090†	20/20/60 (0) 369†
10	M	61	IIA	IgG/BJP-κ	VAD × 4 → HD-CPA → HD-Mel		1/59/40 (53) 2570†	3/7/90 (7.5)§‖ 979†	10/18/72 (1) 1060†	60/35/5 (0)¶ 1250†
11	M	51	IIIA	BJ-κ	VAD × 2 → HD-CPA → HD-Mel × 2		1/24/75 (16.5) 7450‡	2/26/72 (13) 6700‡	5/26/69 (6.5) 5120‡	48/48/4 (1)¶ 65‡
12	F	60	IIIA	IgG-κ	VAD × 4 → HD-CPA → HD-Mel		12/64/24 (17.5) 5190†	12/40/48 (4)§‖ 2200†	4/20/76 (14)§ 2710†	5/33/62 (6)¶ 2440†
13	F	60	IIIA	IgA-λ	VAD × 3 → HD-CPA → HD-Mel × 2				4/42/54 (4) 293†	36/36/28 (0)¶ 131†
14	M	49	IIIB	BJ-λ (PCL)	HD-Mel				12/50/38 (3.6) 210‡	15/40/45 (2.2)§ 120‡
15	M	57	IIIA	IgG-κ	HD-Mel				0/16/84 (16) 2370†	24/48/28 (10)¶ 1640†
16	F	80	IIIA	BJ-λ	Thalidomide					7/79/14 (60.5) 19,400‡
17	M	50	IIIA	IgG-κ	Thalidomide					3/34/63 (7.4) 2270†
18	M	66	IIIA	IgG-λ	Thalidomide					15/40/45 (52) 7581†
19	F	63	IIIA	IgA/BJP-κ	Thalidomide					5/75/20 (67) 5140†
20	F	79	IIIA	IgA/BJP-λ	Thalidomide					40/55/5 (18.5) 324†
21	F	63	IIA	IgG/BJP-κ	Thalidomide					2/70/26 (35.5) 3449†

Case No.	Sex	Age	CS	Type	Chemotherapy Regimen	Greipp Morphology: Mature/Intermediate/Immature, % (BM Plasma Cells, %) Serum† or Urinary‡ M Component: Thalidomide
16	F	80	IIIA	BJ-λ	Thalidomide	10/75/15 (10)§ 1050‡
17	M	50	IIIA	IgG-κ	Thalidomide	0/14/86 (7.5)§ 2622†
18	M	66	IIIA	IgG-λ	Thalidomide	0/72/28 (8.5)¶ 4520†
19	F	63	IIIA	IgA/BJP-κ	Thalidomide	1/55/44 (60)§ 3610†
20	F	79	IIIA	IgA/BJP-λ	Thalidomide	0/11/89 (75.5)§ 4620†
21	F	63	IIA	IgG/BJP-κ	Thalidomide	4/88/8 (29.5)¶ 3269†

*Data were collected before and after the indicated chemotherapy regimens (MP, melphalan and predonine; VAD, 0.4 mg/body vincristine, 10 mg/m^2 doxorubicin [Adriamycin], and 40 mg/body dexamethasone for 4 d; HD-CPA, 2.0 g/m^2 cyclophosphamide for 2 d; HD-Mel, 100 mg/m^2 melphalan for 2 d plus peripheral blood stem cell transplantation). BM indicates bone marrow; CS, clinical stage; BJ, Bence Jones; IgG, immunoglobulin G; BJP, Bence Jones protein; PCL, plasma cell leukemia.

†Serum M component data are expressed in mg.

‡Urinary M component data are expressed in mg/d.

§$P < .01$, for increase of multiple myeloma (MM) cells.

‖$P < .01$, for decrease of intermediate MM cells; compared only for the VAD regimen.

¶$P < .01$, for decrease of immature MM cells.

Table 1-2.
Percentages of Myeloma Cells Based on the Marrow Plasma 38 Method (Surface Antigen) before and after Chemotherapies*

	Marrow Plasma 38 (Surface Antigen): Mature/Intermediate/Immature, % ($CD38^{high}$ Cells, n)											
Case No.	I	MP	I	VAD	I	HD-CPA	I	HD-Mel	I	Thalidomide	I	
1	14/75/11 (445)		15/40/45 (136)									
2	10/78/12 (1473)		10/70/20 (269)									
3			3/59/38 (10,265)		1/35/64 (318)							
4			2/2/96 (3754)		4/6/90 (116)							
5			6/59/35 (525)		8/52/50 (733)							
6			7/88/5 (2508)		3/88/9 (938)							
7			7/44/49 (1123)		6/25/69 (190)							
8			5/52/43 (2762)		3/20/77 (472)		4/18/78 (1418)					
9			1/86/13 (8715)		2/85/13 (616)		6/85/9 (930)		11/82/7 (7)			
10			4/85/11 (5736)		3/88/9 (306)		2/86/12 (103)		9/54/37 (9)			
11			12/22/66 (4112)		10/39/51 (1019)		11/31/58 (626)		4/44/52 (58)			
12			25/67/8 (96)		5/27/68 (537)		5/55/40 (1352)		6/32/62 (278)			
13							11/60/39 (216)		8/10/82 (45)			
14							15/58/27 (205)		14/43/43 (29)			
15							5/3/92 (665)		11/37/52 (64)			
16									21/67/12 (556)		20/72/8 (72)	
17									3/19/88 (333)		6/22/72 (734)	
18									8/84/8 (10,188)		2/78/20 (1663)	
19									10/79/11 (718)		7/89/4 (34)	
20									23/66/11 (33)		2/18/80 (13,125)	
21									6/93/1 (2801)		11/88/1 (3506)	

*Marrow plasma 38 is 3-color flow cytometry using the CD38 plasma gating method. Data were collected before and after the indicated chemotherapy regimens (MP, melphalan and predonine; VAD, 0.4 mg/body vincristine, 10 mg/m^2 doxorubicin [Adriamycin], and 40 mg/body dexamethasone for 4 d; HD-CPA, 2.0 g/m^2 cyclophosphamide for 2 d; HD-Mel, 100 mg/m^2 melphalan for 2 d plus peripheral blood stem cell transplantation).

determined according to the staging system of Durie and Salmon [7]. Phenotypic and morphologic analyses were performed before and after 10 cycles of melphalan and predonine (MP) in 2 cases, 3 or 4 cycles of vincristine, doxorubicin, and dexamethasone (VAD) in 10 cases, high-dose cyclophosphamide (HD-CPA) for stem cell harvest after 3 or 4 cycles of VAD in 5 cases, high-dose melphalan (HD-Mel) followed by ASCT in 6 cases, and thalidomide in 6 cases. In all patients, bone marrow (BM) aspiration was performed at diagnosis after informed consent was given.

2.2. Phenotype Classification

Three-color flow cytometry was performed with the CD38 plasma gating method (Marrow plasma 38) (BML, Tokyo, Japan). BM mononuclear cells were isolated from fresh BM as described previously [8]. The isolated cells were stained with the following combinations: (1) fluorescein isothiocyanate–conjugated CD38 (FITC-CD38) (BD Pharmingen, San Diego, CA, USA), peridinin chlorophyll protein–conjugated CD45 (PerCP-CD45) (BD Biosciences, San Diego, CA, USA), allophycocyanin-conjugated CD19 (Immunotech, Marseilles, France), and phycoerythrin-conjugated CD56 (PE-CD56) (Pharmingen); (2) FITC-CD38, PE-MPC1 (JIMR, Takasaki, Japan), and PerCP-CD45; (3) FITC-CD38, PE-CD49e (VLA-5) (Pharmingen), and PerCP-CD45; and (4) FITC-CD38, PE-CD138 (Immunotech), and PerCP-CD45. Membrane immunofluorescence was evaluated with a FACSCalibur flow cytometer (BD Medical Systems, Franklin Lakes, NJ, USA).

2.3. Morphologic Classification

Air-dried BM smears were stained with May-Giemsa stain or Wright stain. One hundred myeloma (plasma) cells were analyzed in each smear, and the whole smear was surveyed in cases with a low number of myeloma (plasma) cells, which occurred especially after HD-Mel therapy followed by ASCT. The morphologic criteria were based on the classification by Greipp et al [2], but the plasmablastic type was included in the immature type. The persons who performed the morphologic classification were not aware of the flow cytometry results before the examination.

2.4. Statistical Analysis

The differences in the proportions of each type of myeloma cell before and after treatment were analyzed. Statistical significance was determined by 1-way analysis using a version of the Student t test (the method of testing the difference between 2 proportions). The minimal level of statistical significance was taken as $P = .05$. We also analyzed the change in the percentage of each type of myeloma cell. Statistical significance was determined by the Student t test, and the minimal level of significance was taken as $P = .05$.

3. Results

The treatment for patients with MM in our hospitals is as follows: MP for patients older than 70 years, VAD (3 or 4

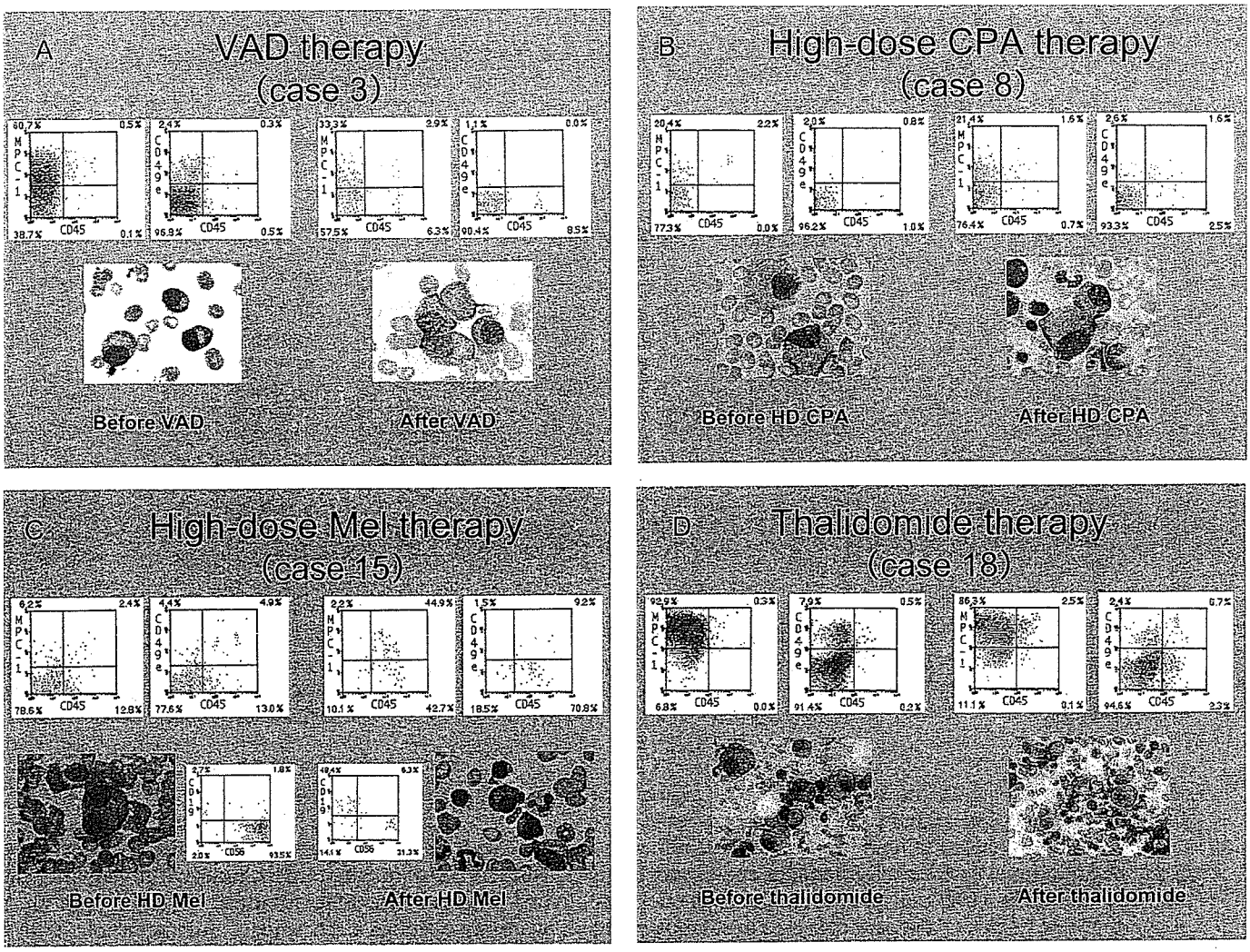

Figure 1. Flow cytometry analysis with the CD38 plasma gating method and May-Giemsa–stained bone marrow aspirates. A, Intermediate myeloma cells ($MPC1^+CD49e^-CD45^-$) were predominant before VAD (vincristine, doxorubicin [Adriamycin], and dexamethasone) chemotherapy, and residual immature myeloma cells ($MPC1^-CD49e^-CD45^{-/+}$) were prominent after VAD treatment. Morphologic findings also confirmed the characteristics of the intermediate and immature myeloma cells. B, Residual intermediate and immature myeloma cells still existed after high-dose (HD) cyclophosphamide (CPA) treatment. Morphologic findings also confirmed the characteristics of immature myeloma cells. C, Residual immature myeloma cells were diminished after HD melphalan (Mel) therapy, and mature myeloma cells ($MPC1^+CD49e^{+/-}CD45^+$) recovered. Interestingly, the mature myeloma cells showed the phenotype of normal plasma cells ($CD19^+CD56^-$). Morphologic findings also confirmed the characteristics of the immature and mature myeloma cells. D, Mature myeloma cells disappeared after thalidomide treatment. Morphologic findings also confirmed the decrease in mature myeloma cells.

cycles) plus HD-CPA for stem cell harvest plus HD-Mel followed by ASCT for patients younger than 70 years, and thalidomide for the refractory patients after completion of these treatments. The patients described in Table 1 underwent analysis for both morphology and phenotype. Analyses before and after VAD chemotherapy or HD-Mel followed by ASCT were performed with 10 and 7 patients, respectively. Consecutive analyses during the course of therapies with VAD, HD-CPA, and HD-Mel followed by ASCT were performed in 4 cases.

In Table 1, we show the percentages of mature, intermediate, and immature plasma (myeloma) cells according to the Greipp classification (Table 1-1) and the Marrow plasma 38 method (Table 1-2). Marrow plasma 38 is a CD38 plasma gating method in which plasma (myeloma) cells are first distinguished from other mononuclear cells on the basis of their strong positivity for CD38 and then classified on the basis of the expression of MPC1 or CD49e in combination with CD45. Representative analyses of samples from patients with different phenotypes are shown in Figure 1. Three or 4 cycles of VAD decreased the total number of myeloma cells and M proteins in the serum or urine of all patients. In particular, the number of intermediate myeloma cells according to the Greipp classification decreased significantly ($P < .01$, 8 of 10 patients). On the other hand, the number of immature myeloma cells relative to the numbers of other types of

myeloma cells increased ($P < .01$, 8 of 10 patients). Therefore, residual immature myeloma cells were more prominent after VAD chemotherapy. These phenomena were confirmed (6 of 10 patients) by Marrow plasma 38 analysis. Intermediate myeloma cells ($MPC1^+CD49e^-CD45^-$) clearly decreased, and residual immature myeloma cells ($MPC1^-CD49e^-CD45^{-/+}$) were detected prominently after VAD chemotherapy (Figure 1A). However, the morphologic and phenotypic results were inconsistent for 2 patients (cases 6 and 10). In these 2 cases, the morphologic analysis showed an increase in immature myeloma cells after VAD therapy, but the phenotype analysis showed an increase of the intermediate type. Although the myeloma cells in most patients with MM are positive for CD56, the myeloma cells in these patients were negative for CD56 and showed a plasmablastic morphology (data not shown).

HD-CPA treatment for the harvest of stem cells after VAD chemotherapy did not show a beneficial effect on the residual immature myeloma cells because those cells either had increased significantly ($P < .01$, 2 of 5 patients) or had stayed unchanged (3 of 5 patients). Marrow plasma 38 analysis also showed the presence of residual intermediate and immature myeloma cells (Figure 1B). Additionally, the percentage of myeloma cells in BM increased in 3 of 5 patients. Regarding the levels of M proteins after HD-CPA treatment, there were small decreases in cases 8 and 9, whereas M-protein levels increased in cases 10 and 12. Therefore, HD-CPA may not be a good treatment for reducing the numbers of myeloma cells.

HD-Mel followed by ASCT was performed in 7 patients, including 1 patient with plasma cell leukemia. This treatment decreased the numbers of immature myeloma cells significantly ($P < .01$, 5 of 7 patients). Of note is that the immature myeloma cells recognized prominently after 3 or 4 cycles of VAD chemotherapy decreased significantly with this treatment. In case 15, most of the immature myeloma cells ($MPC1^-CD49e^-CD45^{-/+}$) disappeared after this treatment (Figure 1C). Interestingly, most residual plasma cells showed the $CD38^{++}CD19^+CD56^-$ phenotype (the phenotype of normal plasma cells) after this treatment.

Although we analyzed only 2 patients, the total number of myeloma cells and the M-protein levels decreased after 10 cycles of MP chemotherapy.

Finally, treatment with thalidomide induced a response in 3 of 6 patients, as shown by the decreases in M-protein levels (cases 16, 18, and 19). However, thalidomide treatment proved not to be useful for reducing immature myeloma cell numbers, because these cells significantly increased after thalidomide treatment ($P < .01$, 4 of 6 patients).

Besides analyzing the numbers of myeloma cells, we also analyzed the changes in the percentages of immature-, intermediate-, and mature-type myeloma cells before and after each type of chemotherapy (Figure 2), and we found similar results, as is shown in Table 1. There were statistically significant increases in the percentages of immature cells ($P = .011$) and decreases in the percentages of intermediate cells ($P = .005$) after VAD chemotherapy, and there were significant decreases in immature cells ($P = .050$) and significant increases in mature cells ($P = .013$) after HD-Mel followed by ASCT.

4. Discussion

The purposes of this study were, first, to find a suitable chemotherapy for MM as shown by the effects on subclasses of myeloma cells and, second, to examine whether analysis by flow cytometry could substitute for the Greipp classification method. So far, total therapy with tandem transplantation has been the most effective chemotherapy for prolonging a complete remission. However, approximately half of patients with MM are not eligible to receive such high-dose chemotherapy because of their age or the impairment of organs. If we can make patients with MM stay in the plateau phase, the overall survival rate will improve. In other words, maintenance therapy could be important for suppressing a recurrence in MM. One of the reasons for difficulties in curing MM patients is believed to be the heterogeneity of myeloma cells. In MM patients, myeloma cells consist of a heterogeneous population with differences in morphology, phenotype, and biological characteristics. It is possible to predict some biological characteristics by the phenotype. For instance, only $CD45^+$ immature myeloma cells proliferate in response to interleukin 6, because src family protein tyrosine kinases, the most important substrates for CD45 protein tyrosine phosphatase, are activated in $CD45^+$ but not in $CD45^-$ myeloma cell lines [6].

We tried to find a suitable treatment for patients according to their major population of myeloma cells. However, consecutive analyses of the biological characteristics of the residual myeloma cells during the course of therapy are usually difficult. We have been searching for an indicator of the progressive disease, relapse, or plateau phase and for a suitable treatment for each situation.

The results of our analyses suggested that a regimen of 3 or 4 cycles of VAD chemotherapy plus HD-Mel followed by ASCT is a reasonable treatment for patients with MM because if the major population of myeloma cells is of the mature or intermediate type, treatment with VAD could be effective in reducing the total population of myeloma cells and the refractory immature myeloma cells could then be diminished by HD-Mel treatment followed by ASCT. However, we also have to consider a method of stem cell harvest other than with HD-CPA, because this treatment is not expected to reduce the residual myeloma cells and overcome complications. Using HD-CPA for peripheral blood stem cell mobilization has been a standard method [9]. Because high-dose etoposide treatment has shown less of an antimyeloma effect, even though this therapy was more efficient for inducing stem cells [10], and EDAP (etoposide, dexamethasone, cytarabine, cisplatin) treatment has been included to target more immature tumor cells [11], it would be better to perform the mobilization after EDAP treatment. Given that Greipp et al mentioned that the residual plasmablastic myeloma cells after ASCT were an independent predictor of poor survival rate [3], the critical point in the treatment of MM might be how to diminish the numbers of immature (plasmablastic) myeloma cells.

Regarding the possible effect of melphalan on myeloma cells, MP is also expected to be a useful treatment to reduce the numbers of immature myeloma cells. Thus, MP is an old but reasonable treatment for MM. As for thalidomide,

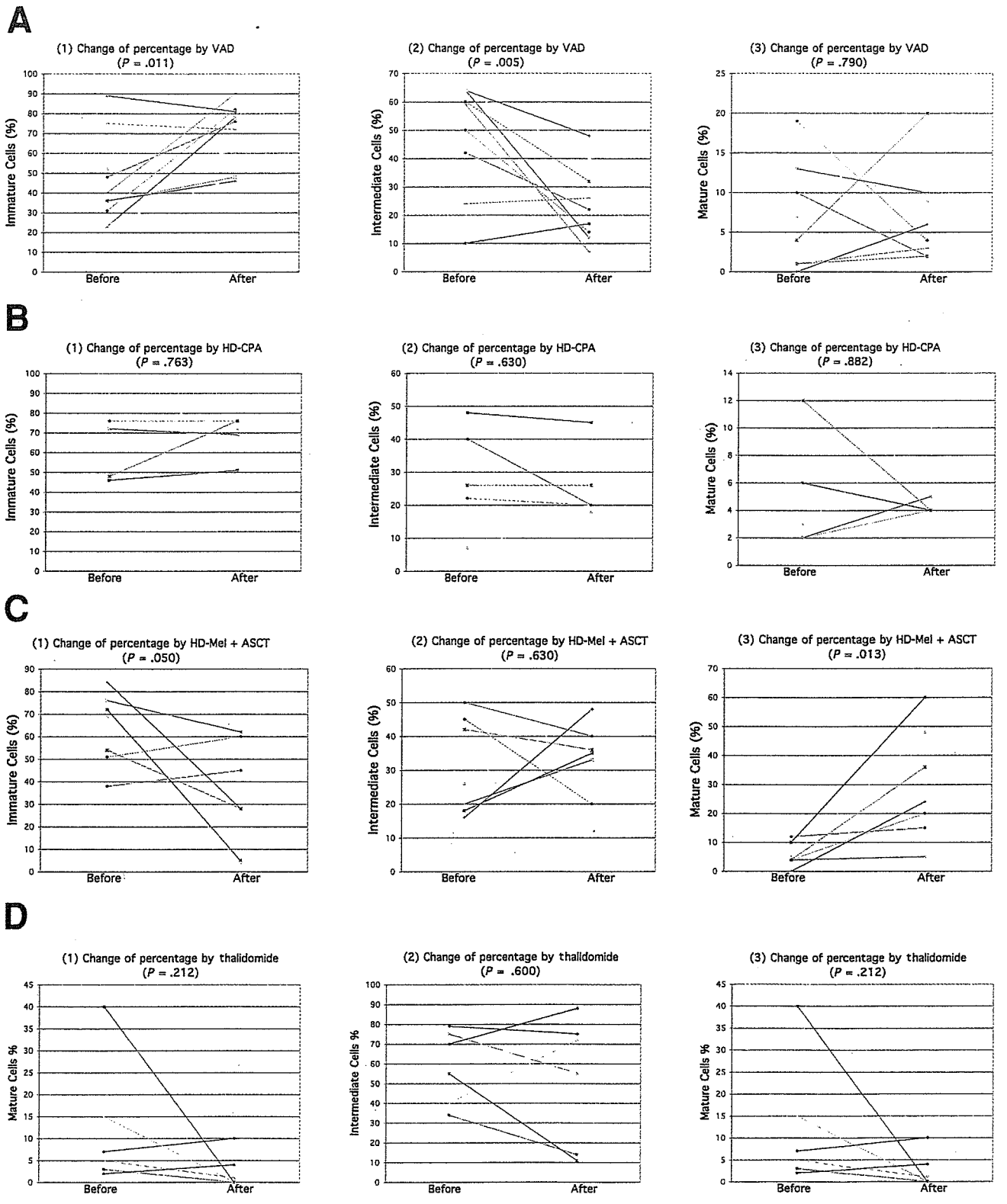

Figure 2. Changes in the percentages of immature- (1), intermediate- (2), and mature-type (3) myeloma cells before and after VAD (vincristine, doxorubicin [Adriamycin], and dexamethasone) chemotherapy (A), high-dose cyclophosphamide (HD-CPA) therapy (B), high-dose melphalan therapy followed by autologous stem cell transplantation (HD-Mel + ASCT) (C), and thalidomide treatment (D). There were statistically significant increases of immature cells ($P = .011$) and significant decreases of intermediate cells ($P = .005$) after VAD chemotherapy, and there were significant decreases of immature cells ($P = .050$) and increases of mature cells ($P = .013$) after HD-Mel + ASCT. However, there was no significant change after thalidomide treatment.

because the effect of thalidomide on patients with refractory MM has been confirmed [12,13], its effect might be best on mature myeloma cells, as we previously reported [14].

In this study, we also investigated whether Marrow plasma 38 analysis could substitute for the Greipp classification. For the most part, the findings of the Marrow plasma 38 analysis were in accord with those of the Greipp classification; however, there were some causes of inconsistency between them. One was the small number of myeloma cells, especially after treatment with HD-Mel followed by ASCT (cases 9, 10, 11, and 13). We think that this inconsistency is reasonable because analyzing a small number of cells by flow cytometry is generally difficult. Second, immature myeloma cells contained many plasmablastic types (cases 2 and 6) or they were negative for CD56 (cases 1 and 10) (data not shown). Therefore, even though the morphologic analysis demonstrated the existence of numerous immature myeloma cells, the phenotype analysis detected them as an intermediate type. Although the relationship between plasmablastic morphology and negativity for CD56 in myeloma cells has already been reported [15,16], we cannot explain the inconsistency between the morphologic and phenotypic findings in these myeloma cells.

In conclusion, a regimen of 3 or 4 cycles of VAD chemotherapy plus HD-Mel treatment followed by ASCT was a reasonable treatment for patients with MM. In particular, HD-Mel could be a critical treatment for reducing the numbers of immature myeloma cells. In addition, we can say that the Greipp classification is a good basis for analysis but that Marrow plasma 38 analysis is an easier method by which to follow the effect of MM treatment.

Acknowledgments

The authors thank S. Fukumoto, N. Nakaju, R. Yamaguchi, K. Yamamoto, and H. Sumida for excellent technical assistance. The authors also thank Dr. K. Sato (Department of Environmetrics and Biometrics, Research Institute for Radiation Biology and Medicine, Hiroshima University) for excellent statistical analysis.

References

1. Moreau P, Facon T, Leleu X, et al. Recurrent 14q32 translocations determine the prognosis of multiple myeloma, especially in patients receiving intensive chemotherapy. *Blood.* 2002;100:1579-1583.
2. Greipp PR, Raymond NM, Kyle RA, O'Fallon WM. Multiple myeloma: significance of plasmablastic subtype in morphological classification. *Blood.* 1985;65:305-310.
3. Greipp PR, Leong T, Bennett JM, et al. Plasmablastic morphology—an independent prognostic factor with clinical and laboratory correlates: Eastern Cooperative Oncology Group (ECOG) myeloma trial E9486 report by the ECOG Myeloma Laboratory Group. *Blood.* 1998;91:2501-2507.
4. Huang N, Kawano MM, Harada H, et al. Heterogeneous expression of a novel MPC-1 antigen on myeloma cells: possible involvement of MPC-1 antigen in the adhesion of mature myeloma cells to bone marrow stromal cells. *Blood.* 1993;82:3721-3729.
5. Kawano MM, Huang N, Harada H, et al. Identification of immature and mature myeloma cells in the bone marrow of human myelomas. *Blood.* 1993;82:564-570.
6. Ishikawa H, Tsuyama N, Kawano MM. Interleukin-6-induced proliferation of human myeloma cells associated with CD45 molecules. *Int J Hematol.* 2003;78:95-105.
7. Durie BG, Salmon SE. A clinical staging system for multiple myeloma: correlation of measured myeloma cell mass with presenting clinical features, response to treatment, and survival. *Cancer.* 1975;36:842-854.
8. Sakai A, Kawano MM, Tanabe O, Kuramoto A. A possible mechanism of inability of immunoglobulin heavy-chain production in Bence-Jones type myeloma cells. *Int J Hematol.* 1993;59:31-40.
9. To LB, Shepperd KM, Haylock DN, et al. Single high doses of cyclophosphamide enable the collection of high numbers of hemopoietic stem cells from the peripheral blood. *Exp Hematol.* 1990;18:442-447.
10. Gianni AM, Bregni M, Siena S, et al. Granulocyte-macrophage colony-stimulating factor or granulocyte colony-stimulating factor infusion makes high-dose etoposide a safe outpatient regimen that is effective in lymphoma and myeloma patients. *J Clin Oncol.* 1992;10:1955-1962.
11. Barlogie B, Velasquez WS, Alexanian R, Cabanillas F. Etoposide, dexamethasone, cytarabine, and cisplatin in vincristine, doxorubicin, and dexamethasone-refractory myeloma. *J Clin Oncol.* 1989;7:1514-1517.
12. Alexanian R, Dimopoulos M. The treatment of multiple myeloma. *N Engl J Med.* 1994;330:484-489.
13. Myeloma Trialists' Collaborative Group. Combination chemotherapy versus melphalan plus prednisone as treatment for multiple myeloma: an overview of 6,633 patients from 27 randomized trials. *J Clin Oncol.* 1998;16:3832-3842.
14. Okikawa Y, Sakai A, Takimoto Y, et al. Progressive myeloma after thalidomide therapy in a patient with immature phenotype of myeloma (plasma) cells. *Int J Hematol.* 2004;79:364-368.
15. Sahara N, Takeshita A, Shigeno K, et al. Clinicopathological and prognostic characteristics of CD56-negative multiple myeloma. *Br J Haematol.* 2002;117:882-885.
16. Sahara N, Takeshita A. Prognostic significance of surface markers expressed in multiple myeloma: CD56 and other antigens. *Leuk Lymphoma.* 2004;45:61-65.

SINGLE-MOLECULE IMAGING OF PROTEIN IN LIVING CELLS BY PIN-FIBER VIDEO-MICROSCOPY

Y HIRAKAWA[1], T HASEGAWA[1], T MASUJIMA[1], M TOKUNAGA[2], N TSUYAMA[3], M KAWANO[3]

[1] *Dept of Frontier Medical Science, Hiroshima University, 1-2-3 Kasumi, Hiroshima 734-8551, Japan*

[2]*Structural Biology Center, National Institute of Genetics, Mishima, Shizuoka 411-8540, Japan,*

Research Center for Allergy and Immunology, RIKEN, Yokohama, Kanagawa 230-0045, Japan

[3]*Dept of Bio-Signal Analysis, Yamaguchi University, 1-1-1 Minami-kogushi, Ube, Yamaguchi 755-8505, Japan*

Email: yhirakaw@hiroshima-u.ac.jp

INTRODUCTION

A single molecule imaging technique is an attractive method which can reveal micro-kinetics of biological molecules. By using this technique, remarkable results have so far been reported.[1-3] In these results, the technique of near-field illuminations, which utilize total internal reflection or a microscopic optical aperture, was adopted. Near field methods need an interface to generate evanescent light illuminating the samples. As the result, the region which can be observed by this technique is sometimes restricted. In order to overcome this point, our group have proposed a novel microscope system of "pin-fiber video-microscope" and reported its applications.[4-6] This system has a unique illumination source consisted of a single optical fiber. With this single fiber system, a selectable region, intensity and area of irradiation in a sample on a microscope are possible by changing the position of the fiber output. In this report, we present single molecular imaging of proteins in a living cell by pin-fiber video-microscope. Kinetic behaviour of proteins caused by extracellular stimulation was visualized. It was found that by analyzing the single molecule images of protein, this new video-microscope has a potential to reveal kinetics of intercellular proteins.

METHODS

In the experiments, signal transducer and activator of transcription 1 (STAT1), in HeLa cells was selected for the visualized target. The experimental setup is depicted in Fig. 1. The most characteristic point of pin-fiber video-microscope is that its light source needs no interface, because it does not utilize evanescent light.

Instrumentation

A coherent radiation from a laser (473 nm, 5 mW, Crystal Laser, Model BCL-005-M) was injected into a single optical fiber (Thorlabs, SM500) with a coupling lens (Thorlabs, A390TM-A). The illuminated region and area were controlled by a micro-manipulator (Narishige, NHN-21 and NHW-4) holding the fiber output. A

fluorescent image from a sample on the microscope (Zeiss, Axioplan) was optically filtered by passing through an interference filter and a notch filter. For elimination of unnecessary fluorescent light from unfocused planes, total optical system of the microscope was changed to a confocal system by setting an additional optical system which consisted of two convex lenses and one pinhole in front of the detector. The noise-reduced fluorescent signal was monitored by a high sensitive CCD camera (Hamamatsu, C7190) and recorded on a digital video recorder (Sony, DSR-30). The recorded digital images were processed and analyzed by computer software (Apple, iMovie; National Institute of Health, NIH images; and Adobe, Photoshop).

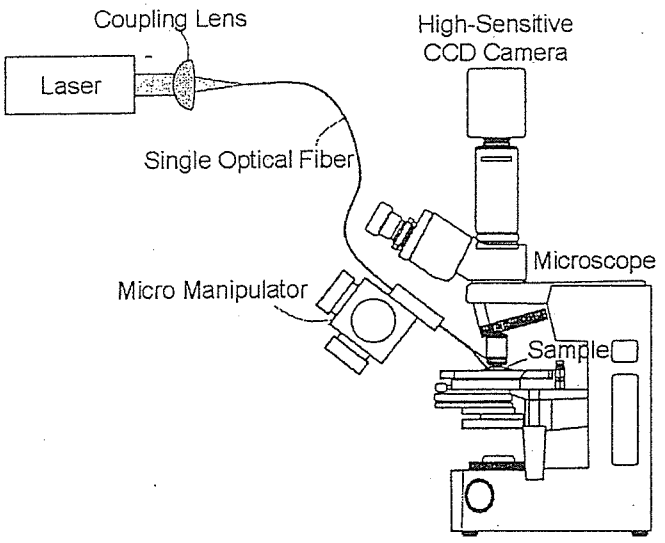

Figure 1. Experimental setup

Sample preparations

STAT1 is one of transcription factor proteins and it is activated by stimulation of interferon (IFN) γ. For visualizing this protein, cDNA encoding STAT1 was fused to green fluorescent protein (GFP) gene by recombination, and STAT1-GFP expression plasmid was transfected into living HeLa cells. In order to suppress background level of images for single molecular imaging, the degree of expression of STAT1-GFP fusion protein was reduced to the level that no fluorescent signals were detected by normal fluorescent microscope mode with a normal CCD camera instead of the high-sensitive CCD camera.

RESULTS

By confirming single step bleaching of fluorescent signals, condition of single molecular imaging was established. With focusing on cell membrane, STAT1-GFPs were recognized as small bright spots when they were recruited to IFN γ receptors after IFN γ stimulation. STAT1 is phosphorylated by tyrosine kinase complex with IFN γ receptor and forms a homodimer. A great number of bright fluorescent spots

appeared and rapidly disappeared one after another. Fig. 2 indicates one of the typical still images of this phenomenon. The fact that wide area can be visualized under single molecular imaging condition is one of the merits of pin-fiber video-microscope.

By focusing on a particular STAT1-GFP spot and analyzing the time course of the recorded images, it was found that different behavior types of STAT1-GFP image intensity existed. The results are shown in Fig. 3. One type was that after appearance of single STAT1 spot, spot brightness was enhanced by a factor of 2 (Fig. 3 (a)). In this case, it might be visualized that one STAT1-GFP came to a receptor first, and after a few hundred ms, another STAT1-GFP was recruited to the same receptor, then these two STAT1-GFPs were dimerized together. The other type was that the STAT1-GFP spot intensity was rapidly increased to this twice brightness (Fig. 3 (b)). This might mean that two STAT1-GFPs were recruited simultaneously to a receptor and they were dimerized. The weak intensity curve labelled with "Single" in Fig. 3 might correspond to STAT1-GFP which did not dimerize or dimerized with non-fluorescent endogenous STAT1. Although this different type of temporal variation of STAT1-GFP fluorescence needs to be investigated further, these preliminary results suggest that pin-fiber video-microscope has a potential to analyze kinetics of intracellular molecules including proteins by using single molecular images.

In conclusion, single molecular observation of protein inside a living cell was tried by pin-fiber video-microscope. Under single-molecule imaging conditions tested, appearance and disappearance of STAT1-GFP spots was clearly observed probably due to phosphorylation mediated activation of STAT1 that resulted in its nuclear translocation from cytoplasm through the cell membrane. Because the two-fold increase in brightness might indicate dimerization of STAT1, this fact suggest that the kinetics of STAT1 dimerization could be observed by this novel method.

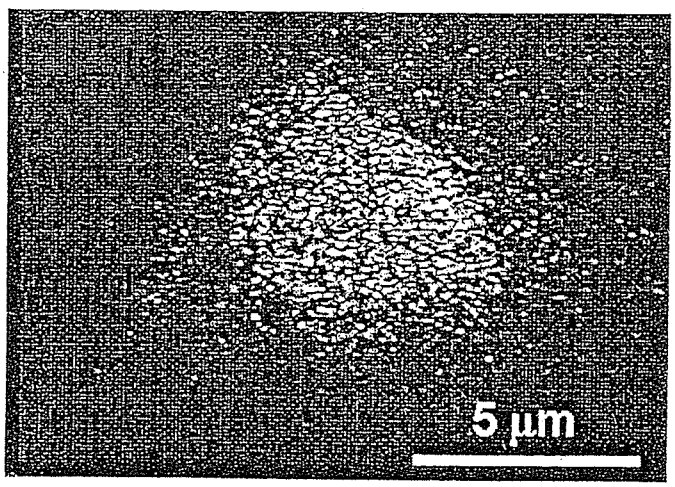

Figure 2. STAT1-GFP single molecule spots visualized by wide area illumination

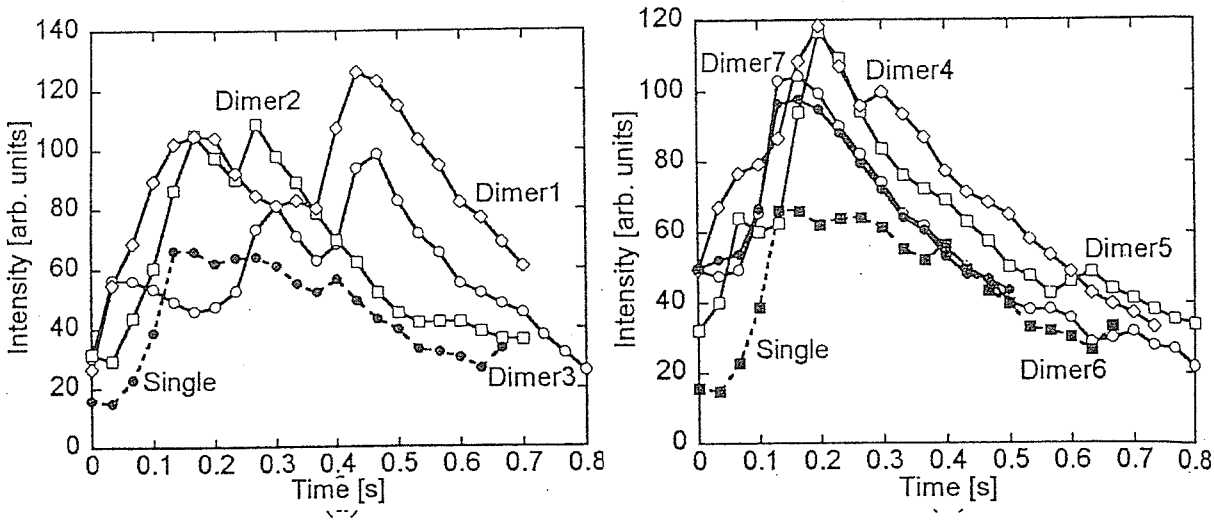

Figure 3. Two-types of temporal variations of STAT1 fluorescent spots intensities

(a) **(b)**

ACKNOWLEDGEMENTS

This research was partially supported by the Japan Ministry of Education, Culture, Sports, Science and Technology, Grant-in-Aid for Scientific Research.

REFERENCES

1 Funatsu T, Harada Y, Tokunaga M, Saito K, Yanagida T. Imaging of single fluorescent molecules and individual ATP turnovers by single myosin molecules in aqueous solution. Nature 1995: 374; 555-9.

2 Weiss S. Fluorescence spectroscopy of single biomolecules. Science 1999: 283; 1676-83.

3 Xu X, Yeung ES. Direct Measurement of single-molecule diffusion and photodecomposition in free solution. Science 1997: 275; 1106; Chemical characterization of single cells and single molecules. Trends in analytical Sciences 1997: 1; 173-81 (http://neo.pharm.hiroshima-u.ac.jp/tals/).

4 Hirakawa Y, Suzutoh M, Ohnishi H, Shingaki T, Eyring EM, Tokunaga M, Masujima T. Analysis of the nano-kinetic movement of a single DNA by a pin-fiber video scope. Anal Sci 2002: 18; 1293-4.

5 Suzuto M, Hirakawa Y, Ohnishi H, Tachino S, Shingaki T, Eyring EM, Masujima T. Nano-kinetics of probe-particles in solution visualized by a pin-fiber video scope. Anal Sci 2003: 19; 43-7.

6 Hirakawa Y, Suzuto M, Ohnishi H, Shingaki T, Eyring EM, Tokunaga M, Masujima T. Observation and analysis of single DNA nano-kinetics by Pin-Fiber Video Scope. Analyst 2003: 128; 676-80.

Bulletin of Informatics and Cybernetics, Vol. 37, 2005

A FAMILY OF REGRESSION MODELS HAVING PARTIALLY ADDITIVE AND MULTIPLICATIVE COVARIATE STRUCTURE

By

Hirokazu YANAGIHARA* and Megu OHTAKI†

Abstract

We propose a new parametric regression model, *Hybrid Linear Regression Model* (or simply HLRM), which has partially additive and multiplicative covariate structure. In an ordinary linear regression model or generalized linear model, it is assumed that the covariates have either an additive or multiplicative effect on the response. A family of HLRM includes an ordinary linear regression model, logarithmic linear model and generalized linear model with normal errors as special cases. In analysis of HLRM, estimating unknown parameters or searching for the best fitting optimal model, we assume the log-normal distribution. Some illustrative analyses applying HLRM to actual data sets are also demonstrated.

Key Words and Phrases: Additive structure, Generalized linear model, Multiplicative structure, Log-normal distribution, Parametric regression model.

1. Introduction

Since the ordinary linear model and the generalized linear model take the simple and convenient forms of their covariates for ease of mathematical treatment, they are universally applicable (see e.g., McCullagh and Nelder (1989)). As these models assume that all of the covariates have either additive or multiplicative effects on the response, we can not analyze data when at the same time some covariates have an additive and others have a multiplicative contribution. However, a common structure for all covariates are not always the best way to express the response value. Actually, on a housing price data in Takahashi et al. (2000), we had better consider that the lot size or a size of building contribute additively on the price, on the other hand, a distance from city center or an age of building contribute multiplicatively on the price. Therefore, we propose a new parametric regression model that has a partially additive and multiplicative structure in the covariates. Let a response variable Y be transformed to a positive value by a known positive non-decreasing function $g(\cdot)$ and a transformed response variable $g(Y)$ have p explanatory variables $(X_1, \ldots, X_p)$ with an additive contribution and q explanatory variables $(Z_1, \ldots, Z_q)$ with a multiplicative contribution. Then independent sets of

* Department of Social Systems and Management, Graduate School of Systems and Information Engineering, University of Tsukuba 1-1-1 Tennodai, Tsukuba, Ibaraki 305-8573, Japan. tel +81–29–853–6451 yanagi@sk.tsukuba.ac.jp

† Department of Environmetrics and Biometrics, Research Institute for Radiation Biology and Medicine, Hiroshima University 1-2-3 Kasumi, Minami-ku, Hiroshima 734-8553, Japan. tel +81–82–257–5852 ohtaki@hiroshima-u.ac.jp